Human Molecular Genetics, 2017, Vol. 26, No. 22 4352–4366

doi: 10.1093/hmg/ddx321
Advance Access Publication Date: 14 August 2017
Original Article

ORIGINAL ARTICLE

Impaired axonal retrograde trafficking of the retromer complex augments lysosomal deficits in Alzheimer's disease neurons

Prasad Tammineni†, Yu Young Jeong†, Tuancheng Feng, Daniyal Aikal and Qian Cai*

Department of Cell Biology and Neuroscience, Rutgers, The State University of New Jersey, Piscataway, NJ 08854, USA

*To whom correspondence should be addressed. Tel: +1 8484451633; Fax: +1 7324451794; Email: cai@biology.rutgers.edu

Abstract

Lysosomal proteolysis is essential for the quality control of intracellular components and the maintenance of cellular homeostasis. Lysosomal alterations have been implicated as one of the main cellular defects contributing to the onset and progression of Alzheimer's disease (AD). However, the mechanism underlying lysosomal deficits in AD remains poorly understood. Here, we reveal that lysosomal deficits are attributed to retromer dysfunction induced by altered retromer trafficking in the axon of AD-related mutant human amyloid precursor protein (hAPP) transgenic (Tg) mouse neurons. We demonstrate that retrograde transport of retromer is impaired, leading to its significant reduction in the soma and abnormal retention within late endosomes in distal axons of mutant hAPP neurons. Therefore, retromer-mediated endosome-to-Golgi retrieval of cation-independent mannose-6-phosphate receptors (CI-MPR) in the soma is disrupted in mutant hAPP neurons, causing defects in lysosome biogenesis. Such defects result in protease deficiency in lysosomes and impaired lysosomal proteolysis, as evidenced by aberrant accumulation of sequestered substrates within lysosomes. Intriguingly, enhancement of retrograde transport in mutant hAPP neurons facilitates the trafficking of axonal retromer toward the soma and thus enhances protease transport to lysosomes, thereby restoring lysosomal proteolytic activity. Taken together, our study provides new insights into the regulation of retromer trafficking through retrograde axonal transport to fulfil its function in promoting lysosome biogenesis in the soma, suggesting a potential approach for rescuing lysosomal proteolysis deficits in AD.

Introduction

As the primary catabolic compartment, the lysosome has been established to receive and degrade biomacromolecules from the secretory, endocytic, autophagic and phagocytic membrane trafficking pathways through the concerted action of acidic hydrolases (1,2). The lysosome requires continuous replenishment of newly synthesized hydrolases to maintain lysosomal degradation capacity. Impaired lysosomal proteolysis forces cells to store cytotoxic cargos, such as pathological protein aggregates and dysfunctional organelles, thus triggering apoptotic cascades and cell death (3). Lysosomal deficits have been linked to the pathogenesis of Alzheimer's disease (AD) (4,5). However, the underlying mechanism of such deficits in AD remains poorly understood.

The retromer complex has been established as a key molecular factor responsible for the retrieval of cargo receptors from the endosome to the trans-Golgi network (TGN) (6–8). As a multimeric protein complex, retromer is composed of a sorting nexin (SNX) heterodimer and a vacuolar protein sorting (VPS)

†These authors contributed equally to this work.
Received: June 16, 2017. **Revised:** August 2, 2017. **Accepted:** August 9, 2017

heterotrimer (9). The intramembranous acid hydrolase receptor—cation-independent mannose-6-phosphate receptor (CI-MPR), a well-characterized cargo sorted by retromer—transports newly synthesized lysosomal enzymes from the TGN to the endosomal compartment for their translocation to the terminal destination: the lysosome (6,10). Proper delivery of Cathepsin D and other proteases to the lysosome depends on the presence of CI-MPR in the Golgi. Retromer coordinates this crucial step required for lysosome biogenesis by mediating CI-MPR retrieval from the late endosome to the Golgi (6,10,11).

Neurons, with their distinct functional domains and complex requirements for regulated trafficking, provide a fertile environment in which to study the role of this sorting complex. A number of recent studies have demonstrated that deficiencies in VPS35, a key component of the retromer complex, result in impaired α-amino-3-hydroxy-5-methyl-4-isoxazolepropionic acid (AMPA) receptor trafficking, decreased dendritic spine maturation, a reduction in long-term potentiation (LTP) (12,13). Dopaminergic neuron loss following retromer deficiency has also been observed by impairing mitochondrial fusion and fission or by disrupting endosome-to-Golgi retrieval of lysosome-associated membrane glycoprotein 2a (Lamp2a) (14–16). Moreover, accumulating evidence indicates that retromer deficiency may contribute to the etiology of both AD and Parkinson's disease (PD) (11). In AD, a relative decrease in multiple retromer proteins was found in some disease-affected regions of AD patient brains (17). Reducing retromer proteins was shown to exacerbate memory deficits in a mouse model of the disease (18). Studies have also linked retromer deficiency to the bidirectional modulation of amyloid-β (Aβ) production (7,17–19). Thus, elucidating retromer function in the brain and its regulation are of critical importance for understanding the pathogenesis of AD and PD.

Efficient endocytic transport is fundamental to the maintenance of cargo trafficking and recycling processes. Transport failure has been noted to lead to missorting and abnormal cargo accumulation (20). The retromer complex is recruited to the late endosome through the interaction of late endosomal Rab7 with the retromer proteins VPS35 and VPS26 (21,22). The late endosome has been consistently shown to co-localize or associate with retromer and other VPS subunits (21,23–25). In neurons, while the TGN is mainly localized in the soma, the late endosome is enriched in the axon and undergoes predominant long-distance retrograde transport toward the soma (26–28). Given that cargo sorting occurs primarily in the soma of neurons, this raises a fundamental question: Does retrograde axonal transport regulate retromer functionality in the soma, in particular, the retromer-dependent endosome-to-Golgi retrieval of CI-MPR? We previously uncovered a cellular defect in AD neurons: retrograde transport of the late endosome is impaired due to dynein-Snapin motor-adaptor uncoupling (26). Thus, a critical question remains: Do such defects compromise retromer trafficking and thus its role in the soma of AD neurons?

Here, we reveal that impaired retrograde transport of retromer in the axon leads to its significant reduction in the soma of mutant hAPP neurons. Therefore, somatic retromer-mediated CI-MPR targeting to the Golgi is disrupted, resulting in defective protease transport to lysosomes and impaired lysosomal proteolysis. Strikingly, enhanced retrograde transport facilitates the trafficking of axonal retromer toward the soma and thus lysosome biogenesis, thereby rescuing lysosomal defects in AD neurons. Our results provide both *in vitro* and *in vivo* evidence that retrograde axonal transport is essential for maintaining retromer's level and functionality in the soma of neurons. Our study establishes a foundation for future investigations into cellular pathways enhancing lysosomal proteolytic activity through the up-regulation of retrograde transport and retromer function in AD.

Results

Impaired trafficking of the retromer toward the soma of mutant hAPP Tg neurons

The retromer complex mediates the retrieval of its cargo—CI-MPR—from the late endosome to the Golgi, which is required for proper transport of proteases to the lysosome (11,29). We examined the intracellular distribution of the core retromer proteins VPS35 and VPS26 in cortical neurons derived from an AD-related mouse model—mutant hAPP transgenic (Tg) mice harboring the human AD Swedish and Indiana mutations of hAPP (J20) (30). We found that the levels of VPS35 and VPS26 were reduced by ∼32% and ∼30% in mutant hAPP Tg neurons relative to those of WT littermate controls ($P < 0.001$), respectively (Fig. 1A and B). It has been shown that Rab7 recruits retromer to the late endosome through direct binding to VPS35 (21,22). Consistently, we demonstrated that the retromer proteins VPS35 and VPS26 along with CI-MPR were detected on Rab7-associated late endosomes immunoisolated from light membrane fractions of mouse brains (Fig. 1C). Previous studies showed that Snapin, a dynein motor adaptor, associates with late endocytic compartments and mediates the recruitment of dynein motors to late endosomes (26,27). Consistent with these observations, we showed that Snapin, along with dynein motor intermediate chain (DIC), was present on Rab7-associated late endosomes (Fig. 1C). Moreover, the purity of the preparation was confirmed by lack of p115 (a Golgi marker) and cytochrome *c* (a mitochondrial marker) (Fig. 1C).

In neurons, late endosomes are relatively abundant in the axon and undergo long-distance retrograde transport toward the soma (26–28,31). We next determined axonal distribution of the retromer. In WT neurons, VPS35 appeared as vesicular structures and partially co-localized with Rab7-associated late endosomes (Fig. 1D). However, in the axon of hAPP neurons, VPS35 was retained within late endosomes, as evidenced by markedly increased association with late endosomes (WT: 57.67% ± 2.80%; hAPP: 80.81% ± 1.88%; $P < 0.001$) (Fig. 1D and E). Consistently, compared to WT neurons, we detected ∼56% and ∼131% increase in the densities of total and late endosome-associated VPS35 in the axon of AD neurons, respectively (total VPS35 per 10 μm axon: 1.56 ± 0.08; $P < 0.001$; late endosomal VPS35 per 10 μm axon: 2.31 ± 0.13; $P < 0.001$) (Fig. 1D and E). In contrast, we found a very small portion of VPS35 associated with late endosomes in the dendrites of WT neurons (8.72% ± 0.79%; $P < 0.001$) (Supplementary Material, Fig. S1A and B). Such results related to dendritic retromer were also reported in previous studies (32,33). It is important to note that there was no detectable difference in terms of the percentage of dendritic VPS35 association with late endosomes between WT and mutant hAPP neurons (hAPP: 10.18% ± 0.84%; $P = 0.214$) (Supplementary Material, Fig. S1A and B). Thus, our observation suggests differential mechanisms of retromer trafficking in the axon versus the dendrite. Given that the TGN is mainly localized in the soma, retrograde axonal transport of late endosomes could be critical for trafficking retromer toward the soma and thus mediating endosome-to-Golgi retrieval of CI-MPR. Axonal late endosomes likely serve as critical carriers executing retromer trafficking, thereby regulating its function in the soma.

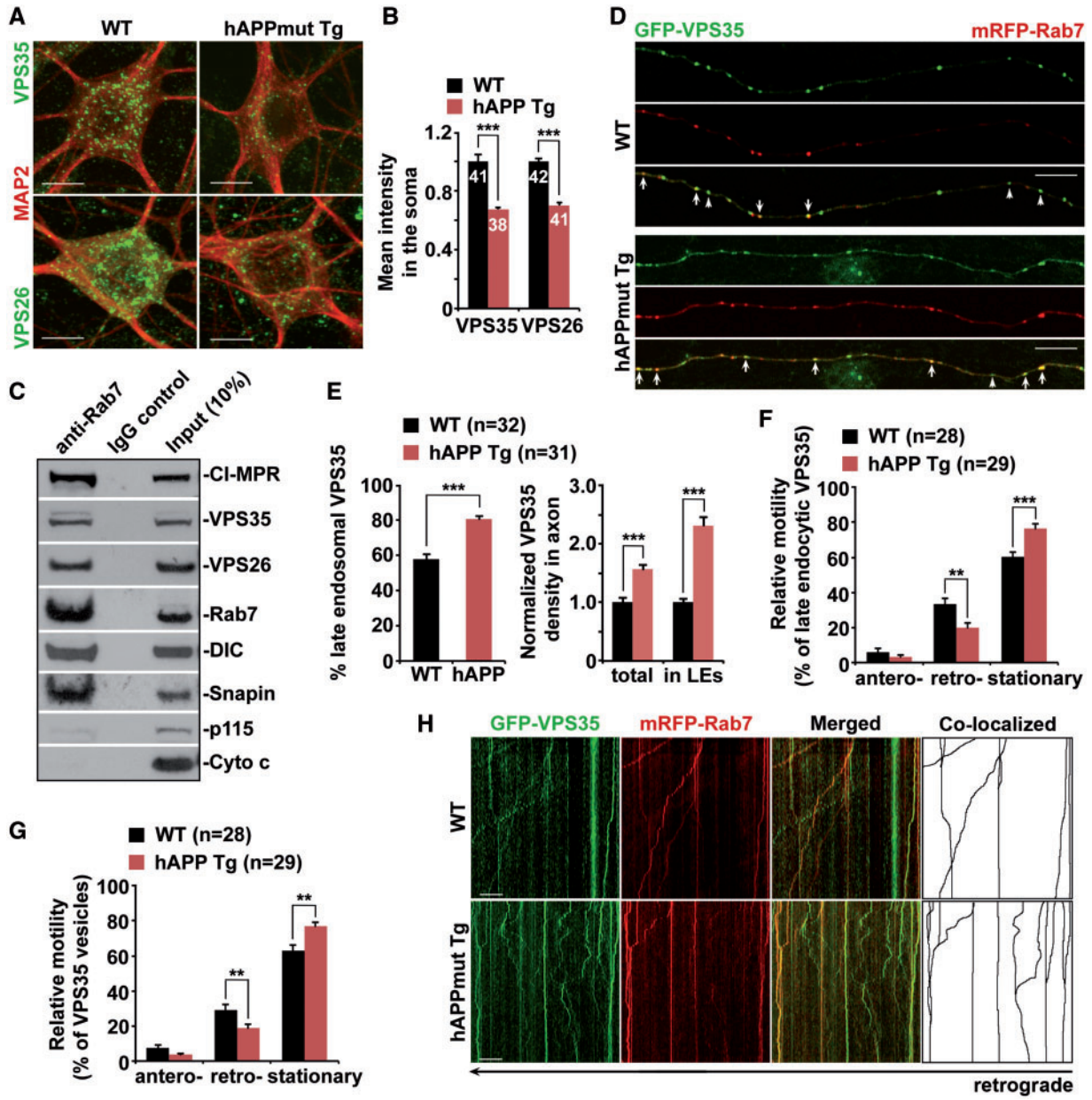

Figure 1. Impaired trafficking of the retromer toward the soma of mutant hAPP Tg neurons. (**A** and **B**) Representative images (A) and quantitative analysis (B) showing reduced targeting of the retromer proteins VPS35 and VPS26 to the soma of mutant hAPP Tg neurons. Note that the densities of somatic VPS35 and VPS26 were significantly reduced in mutant hAPP neurons. The mean intensity of VPS35 or VPS26 in the soma of hAPP neurons was normalized against that of MAP2 from the same neurons and compared to that of WT littermate controls. (**C**) Immunoisolation assay showing association of VPS35, VPS26 and CI-MPR with late endosomes in mouse brains. Rab7-associated late endosomes were immunoisolated with anti-Rab7-coated Dyna magnetic beads from light membrane fractions of mouse brains, followed by sequential immunoblotting on the same membranes after stripping between each antibody application. The purity of the preparation was confirmed by the absence of p115 (a Golgi marker) and cytochrome c (a mitochondrial marker). (**D** and **E**) Representative images (D) and quantitative analysis (E) showing aberrant retention of VPS35 within late endocytic organelles along mutant hAPP Tg axons. Note that the densities of VPS35 and late endosome-associated VPS35 were increased in hAPP axons. While late endosome-loaded VPS35 is marked by arrows, the non-late endosomal VPS35 is indicated by arrowheads. The percentage of VPS35 co-localized with Rab7-labeled late endosomes in the axons of WT and mutant hAPP neurons was quantified. The average numbers of total VPS35 or VPS35 associated with Rab7-labeled late endosomes per 10 μm axon in mutant hAPP neurons were further quantified and normalized to those of WT neurons, respectively (E). (**F–H**) Impaired retrograde transport of late endosome-loaded VPS35 in the axon of mutant hAPP Tg neurons. The relative motility of axonal VPS35 and late endosome-associated VPS35 was measured. Vertical lines represent stationary organelles; oblique lines or curves to the right represent anterograde movements; lines to the left indicate retrograde transport. Cortical neurons were transfected with GFP-VPS35 and mRFP-Rab7 at DIV5, followed by time-lapse imaging at DIV13-15. Note that a significant portion of VPS35 co-localized and co-migrated with late endosomes along the same axon of WT neurons. Data were quantified from a total number of neurons (n) as indicated in parentheses (E, F and G) or on the top of bars (B) from at least four independent repeats. Scale bars: 10 μm. Error bars: SEM. Student's *t* test: $^{***}P < 0.001$; $^{**}P < 0.01$.

To address whether a significant reduction of retromer in the soma and abnormal retention in the axon of mutant hAPP neurons result from impaired retrograde transport, we next assessed the motility of the retromer protein, VPS35, by time-lapse confocal imaging in live neurons. Late endosomes undergo retrograde transport along the axon (27,28,31,34). We demonstrated that a significant portion of VPS35 co-migrated with Rab7-labeled late endosomes in a retrograde direction along the axon of WT neurons. However, in mutant hAPP neurons, the retrograde transport motility of axonal VPS35 was significantly reduced (WT: 29.35% ± 2.81%; hAPP: 18.92% ± 2.22%; $P < 0.01$). Late endosomal VPS35 transport was also impeded along the same axon (WT: 33.52% ± 3.25%; hAPP: 19.90% ± 2.72%; $P < 0.01$). This is consistent with our previous results, which have shown impaired retrograde transport of late endosomes in mutant hAPP axons (26). As an internal control, anterograde transport did not show any detectable changes, suggesting selective defects in retrograde transport of retromer in AD axons (Fig. 1F–H). Consistent with previous studies (32,33), we found that retromer displayed bi-directional short-range movement along the dendrite of WT neurons. Mutant hAPP neurons showed no detectable change in the motility of dendritic retromer relative to WT littermate controls (data not shown). Therefore, our findings indicate that defective retrograde transport leads to abnormal late endosomal retention of retromer in distal axons, thereby disrupting its trafficking toward the soma in AD neurons.

Reduced density of somatic retromer in mutant hAPP Tg mouse brains

To confirm our imaging data from cultured neurons, we analyzed the distribution of the retromer in mutant hAPP Tg mouse brains. In the hippocampal mossy fibers of WT mice, the retromer protein VPS35 appeared as dim vesicles or a background-like pattern. However, in the same regions of AD mice, VPS35 was observed as clusters (averaged number of VPS35 clusters per imaging slice section: WT: 10.84 ± 0.66; hAPP: 28.13 ± 2.03; $P < 0.001$) (Fig. 2A and C). Given that hippocampal mossy fibers are enriched with axons and presynaptic terminals, VPS35 clusters in mutant hAPP Tg mice were partially co-localized with synaptophysin (SYP)-labeled presynaptic terminals (Fig. 2A). The density of synaptic VPS35 clusters was significantly increased in mutant hAPP Tg mice compared to that of WT littermate controls (averaged number per imaging slice section: WT: 5.38 ± 0.52; hAPP: 20.08 ± 2.15; $P < 0.001$) (Fig. 2A and D). These VPS35 clusters also showed increased association with Rab7-labeled late endosomes in the hippocampal mossy fibers of hAPP mice (averaged number per imaging slice section: WT: 9.05 ± 0.72; hAPP: 31.57 ± 1.12; $P < 0.001$) (Fig. 2B and D). Furthermore, late endosomal retromer was retained in dystrophic presynaptic terminals surrounding amyloid plaques (Fig. 2B). Consistent with our imaging data from neuron cultures (Fig. 1A and B), somatic retromer protein VPS35 was found to be significantly reduced in the hippocampal regions of mutant hAPP Tg mice compared to that of WT littermate controls (0.72 ± 0.01; $P < 0.001$) (Fig. 2E and F). Thus, these *in vitro* and *in vivo* observations consistently showed aberrant accumulation of retromer in distal axons and a significant reduction in the soma of mutant hAPP neurons. Moreover, there is no detectable reduction in VPS35 levels in both mutant hAPP Tg neurons and mouse brains compared to WT littermates (Neuron: 0.91 ± 0.07; $P = 0.22$; Brain: 1.05 ± 0.1; $P = 0.59$) (Supplementary Material, Fig. S2). Also, the expression levels of CI-MPR and Snapin were not altered in mutant hAPP mouse neurons and brains (CI-MPR: Neuron: 1.12 ± 0.09; $P = 0.26$; Brain: 0.97 ± 0.08; $P = 0.73$; Snapin: Neuron: 1.01 ± 0.04; $P = 0.90$; Brain: 1.02 ± 0.1; $P = 0.85$) (Supplementary Material, Fig. S2).

Impaired Golgi targeting of CI-MPR in the soma of mutant hAPP Tg mouse neurons

Retromer mediates CI-MPR retrieval from late endosomes to the Golgi (24), acting primarily in the soma of neurons due to predominant somatic localization of the Golgi. We hypothesized that a reduction in somatic levels of retromer may impair its role in mediating CI-MPR targeting to the Golgi in AD neurons. We found that CI-MPR was enriched in the soma of hippocampal neurons in WT mice, but was remarkably reduced in mutant hAPP Tg mice (0.66 ± 0.01; $P < 0.001$) (Fig. 3A and B). Furthermore, Golgi localization of CI-MPR in the soma of hAPP neurons was dramatically decreased compared to that of WT neurons (0.64 ± 0.02; $P < 0.001$) (Fig. 3C and D).

We further examined the intracellular distribution of CI-MPR in cultured mutant hAPP neurons. Consistent with our imaging data from mutant hAPP Tg mouse brains, we detected a decrease in the levels of CI-MPR in the soma of hAPP neurons when compared to those of WT neurons (0.782 ± 0.027; $P < 0.001$) (Supplementary Material, Fig. S3A and B). Moreover, in mutant hAPP neurons, CI-MPR puncta were relatively dispersed and located in the peripheral regions, and its localization in the Golgi was significantly reduced to ~63% (hAPP: 0.629 ± 0.038; $P < 0.001$) (Supplementary Material, Fig. S3C and D). Given that retromer mediates the endosome-to-Golgi retrieval of CI-MPR, our observations consistently suggest that impaired targeting of CI-MPR to the Golgi is attributed to defective functionality of retromer in the soma of mutant hAPP neurons.

Furthermore, we found that CI-MPR was clustered and accumulated within late endosomes at presynaptic terminals of hippocampal regions in mutant hAPP Tg mice. While it was not readily detected in WT mice, the density of CI-MPR clusters co-localized with SYP and Rab7 was robustly increased in hippocampal mossy fibers of mutant hAPP Tg mice (averaged number per imaging slice section: SYP: WT: 5.2 ± 0.39; hAPP: 15.94 ± 1.23; $P < 0.001$; Rab7: WT: 9.14 ± 0.76; hAPP: 22.94 ± 1.04; $P < 0.001$) (Supplementary Material, Fig. S3E, F and G). This result is consistent with undetectable changes in CI-MPR levels observed in both cultured neurons and brains of mutant hAPP mice (Supplementary Material, Fig. S2). Together, our data suggest that impaired retromer trafficking results in retention of its cargo, CI-MPR, within late endosomes in distal regions of AD neurons, thereby disrupting the retrieval of CI-MPR from late endosomes to the Golgi in the soma.

To provide further evidence relevant to AD, we examined synaptosomal preparations in the hippocampal regions of AD patient brains. Strikingly, VPS35 was robustly increased relative to that of control subjects (2.11 ± 0.26; $P < 0.01$) (Supplementary Material, Fig. S4A and B). Similar increases in AD patient brains were detected in the levels of Rab7 (1.37 ± 0.09; $P = 0.01$), but not SYP, a synaptic vesicle protein (1.1 ± 0.08; $P = 0.28$). However, compared to control subjects, the post-nuclear supernatants of AD patient brains did not show such alterations in the levels of VPS35 and Rab7 (VPS35: 0.77 ± 0.14; $P = 0.166$; Rab7: 1.00 ± 0.24; $P = 0.978$) (Supplementary Material, Fig. S4A and B). These

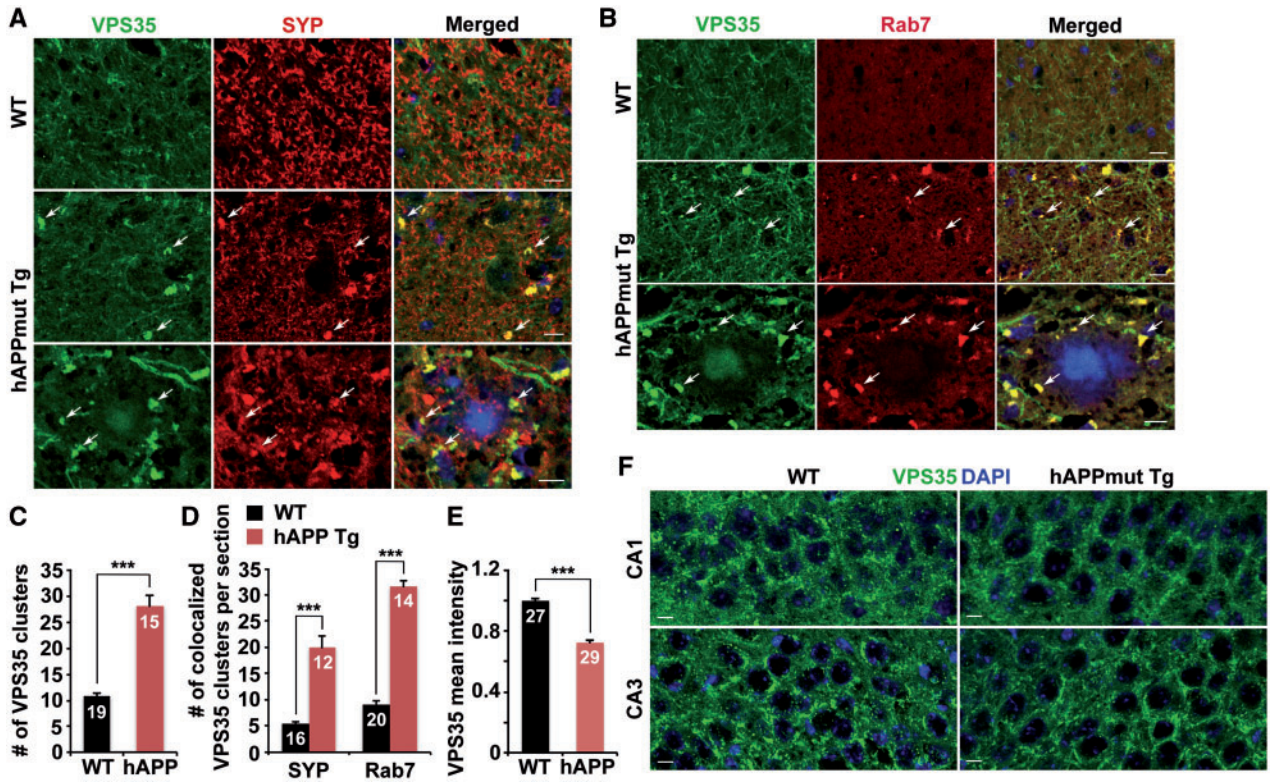

Figure 2. Reduced density of somatic retromer in mutant hAPP Tg mouse brains. (**A–D**) Representative images (A and B) and quantitative analysis (C and D) showing accumulation of the retromer protein VPS35 within late endosomes in hippocampal mossy fibers of mutant hAPP Tg mouse brains. Note that late endosome-loaded retromer was retained within dystrophic presynaptic terminals surrounding amyloid plaques. The average numbers of VPS35 clusters and VPS35 co-localized with SYP or Rab7 in the hippocampal mossy fiber per imaging slice section (320 μm × 320 μm) were quantified, respectively. (**E** and **F**) Reduced density of somatic VPS35 in the hippocampal neurons of mutant hAPP Tg mouse brains. The mean intensity of somatic VPS35 in hippocampal regions per imaging slice section (320 μm × 320 μm) was quantified. Scale bars: 10 μm. Data were quantified from a total number of imaging hippocampal slice sections indicated on the top of bars (C, D and E) from three pairs of mice. Error bars represent SEM. Student's *t* test: $^{***}P < 0.001$.

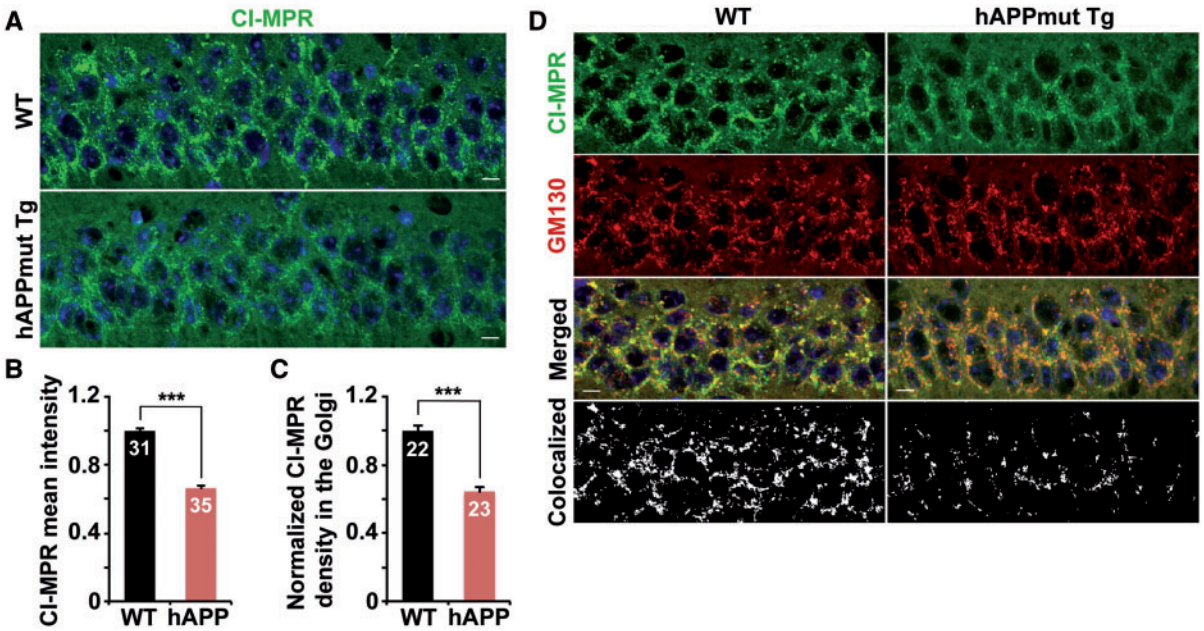

Figure 3. Impaired Golgi targeting of CI-MPR in the soma of mutant hAPP Tg mouse neurons. (**A** and **B**) Reduced density of somatic CI-MPR in the hippocampal neurons of mutant hAPP Tg mouse brains. The mean intensity of somatic CI-MPR in hippocampal regions per imaging slice section (320 μm × 320 μm) was quantified. (**C** and **D**) Quantitative analysis (C) and representative images (D) showing that CI-MPR trafficking to the Golgi is decreased in hippocampal regions of mutant hAPP Tg mice. The Golgi targeting of CI-MPR was expressed as co-localized intensity of CI-MPR with GM130 (a Golgi marker) in the soma of hippocampal neurons. Scale bars: 10 μm. Data were quantified from a total number of imaging hippocampal slice sections indicated on the top of bars (B and C) from three pairs of mice. Error bars represent SEM. Student's *t* test: $^{***}P < 0.001$.

results were quantified from the experiments using four control subjects and five patient brains (postmortem interval 7.08–22.5 h). Thus, the observation from human patient brains is consistent with our imaging data from mutant hAPP Tg mouse brains, suggesting that retromer is aberrantly retained in axonal terminals of AD neurons.

Reduced protease density within lysosomes in mutant hAPP Tg neurons

Proper transport of proteases to the lysosome relies on retromer-mediated retrieval of CI-MPR from the late endosome to the Golgi (11,29). We next examined the intracellular distribution of lysosomes loaded with Cathepsin D (CathD) in cultured primary cortical neurons. Neurons were incubated with Bodipy FL-pepstatin A, which binds to the active site of the mature form of Cathepsin D, followed by immunostaining with antibodies against LAMP-1 and MAP2. While the fluorescence signal of Bodipy FL-pepstatin A was detectable predominantly in the soma, but not in the neuronal processes of neurons revealed by MAP2 staining (Fig. 4A), immunofluorescent signals stained by the anti-Cathepsin D antibody were mostly co-labeled by Bodipy FL-pepstatin A, suggesting that they represent a mature form of active protease with full hydrolytic activity. Moreover, most LAMP-1-indicated lysosomes in the soma co-localized with active Cathepsin D marked by Bodipy FL-pepstatin A (Fig. 4A). This data indicates that active Cathepsin D-enriched lysosomes are preferentially localized in the soma of neurons in which CI-MPR-dependent transport of newly synthesized lysosomal enzymes from the Golgi mainly takes place (6,10).

Compared to those of WT littermate controls, active Cathepsin D labeled by the Bodipy FL-pepstatin A was markedly decreased in cultured mutant hAPP Tg neurons (0.61 ± 0.04; $P < 0.001$) (Fig. 4B and C). Moreover, active Cathepsin D within somatic lysosomes was remarkably reduced to 35% (0.35 ± 0.04; $P < 0.001$) (Fig. 4B and D). To further confirm such lysosomal defects, we also examined the active form of lysosomal Cathepsin B (CathB), which was specifically labeled by the cresyl violet fluorogenic substrate CV-(Arg-Arg)2 (Magic Red). Consistently, normalized mean intensities of the active form of lysosomal Cathepsin B in the soma of mutant hAPP neurons were significantly reduced compared to that of WT littermate controls (0.64 ± 0.02; $P < 0.001$) (Supplementary Material, Fig. S5A and B).

We next determined whether a reduction in VPS35 levels, particularly in the soma of neurons, recapitulates lysosomal defects observed in AD neurons by knocking down VPS35. We found that somatic VPS35 was reduced to ∼64% in WT neurons expressing VPS35-small hairpin RNA (shRNA) relative to those in control shRNA expressed neurons (0.64 ± 0.04; $P < 0.001$) (Fig. 4E and F), suggesting that VPS35-shRNA efficiently reduces endogenous VPS35 levels. Moreover, compared to controls, active lysosomal Cathepsin D labeled by Bodipy FL-pepstatin A was significantly decreased (0.71 ± 0.04; $P < 0.001$) in WT neurons expressing VPS35-shRNA (Fig. 4G and H). In addition, active Cathepsin B levels were also reduced in the soma of neurons following knockdown of VPS35 (0.65 ± 0.03; $P < 0.001$) (Supplementary Material, Fig. S5C and D), which is consistent with our observations from mutant hAPP neurons (Supplementary Material, Fig. S5A and B). Together, these findings indicate that retromer levels in the soma of neurons are critical for the maintenance of lysosomal degradation capacity through facilitating protease transport to lysosomes.

Impaired lysosomal proteolysis in mutant hAPP Tg neurons

We next tested whether protease deficiency in the lysosome results in impaired lysosomal proteolytic activity by assessing dynamic lysosomal proteolysis in live neurons derived from WT and mutant hAPP Tg mice. We investigated lysosomal degradation of epidermal growth factor (EGF) receptor (EGFR) after internalization. Endogenous EGFRs were primarily located on the plasma membrane of neurons before EGF incubation. Following EGF treatment, EGFRs were internalized and clustered into large puncta (Fig. 5A). At 3 h after EGF incubation, the normalized EGFR mean intensity reached peak levels with no detectable difference between WT and hAPP neurons. However, at 7 h after EGF treatment, a significant portion (40.80% ± 2.38%; $P < 0.001$) of internalized EGFRs was degraded in WT neurons, whereas almost all EGFR puncta (91.18% ± 5.46%; $P = 0.243$) remained in the hAPP neurons, suggesting impaired lysosomal degradation (Fig. 5A and B).

We further examined Keima-Mito Red-labeled acidic mitochondria within degradative organelles in live WT and mutant hAPP Tg neurons (35,36). Acidic mitochondria indicated by Keima-Mito Red were mainly detectable in the soma of neurons and co-localized with the lysosome, suggesting that these defective mitochondria are trapped into lysosomes for degradation (Fig. 5C). Compared to WT controls, the number of acidic mitochondria in the soma of mutant hAPP neurons was significantly increased (WT: 16.11 ± 1.95; hAPP: 55.5 ± 3.76; $P < 0.001$) (Fig. 5C and D). These data are consistent with impaired lysosomal proteolysis as a result of reduced luminal proteases in the lysosome, thereby enhancing lysosomal retention of defective mitochondria.

AD-linked lysosomal deficits in mutant hAPP Tg mouse brains

Given that lysosomes enriched with proteases are preferentially localized in the soma of neurons (27,28,31,37) (Fig. 4A), we examined Cathepsin D distribution in mutant hAPP mouse brains. Consistent with our imaging data from cultured mutant hAPP neurons, the density of somatic Cathepsin D was significantly reduced in the hippocampal regions of mutant hAPP Tg mice relative to that of WT littermates (0.54 ± 0.016; $P < 0.001$) at the age of 8 months (Fig. 6A and B). To determine luminal Cathepsin D levels in the lysosome, we quantified the co-localized intensity of Cathepsin D and LAMP-1-labeled lysosomes in the soma of hippocampal neurons from WT and hAPP Tg mice. Compared to WT controls, lysosomal Cathepsin D was markedly decreased in mutant hAPP neurons (0.39 ± 0.018; $P < 0.001$) (Fig. 6C and D). We also examined Cathepsin B and Cathepsin L in the hippocampal regions of mutant hAPP mice, and detected a similar reduction of the densities in the soma relative to WT littermate controls (Cathespin B: 0.65 ± 0.03; $P < 0.001$; Cathespin L: 0.70 ± 0.02; $P < 0.001$) (Supplementary Material, Fig. S6). Luminal levels of Cathepsin B and Cathepsin L within lysosomes were also decreased (data not shown). Thus, a lack of proteases in the lysosome in mutant hAPP neurons could compromise lysosomal proteolysis. We consistently showed that mutant hAPP Tg neurons displayed ∼88% increase in defective mitochondria retained within lysosomes (1.88 ± 0.12; $P < 0.001$) (Fig. 6E and F), suggesting a defective clearance of lysosomal mitochondria. Consistent with our imaging data from cultured mutant hAPP Tg neurons, our *in vivo* observations provide additional lines of evidence that protease deficiency in the lysosome leads to impaired lysosomal proteolytic activity in AD neurons.

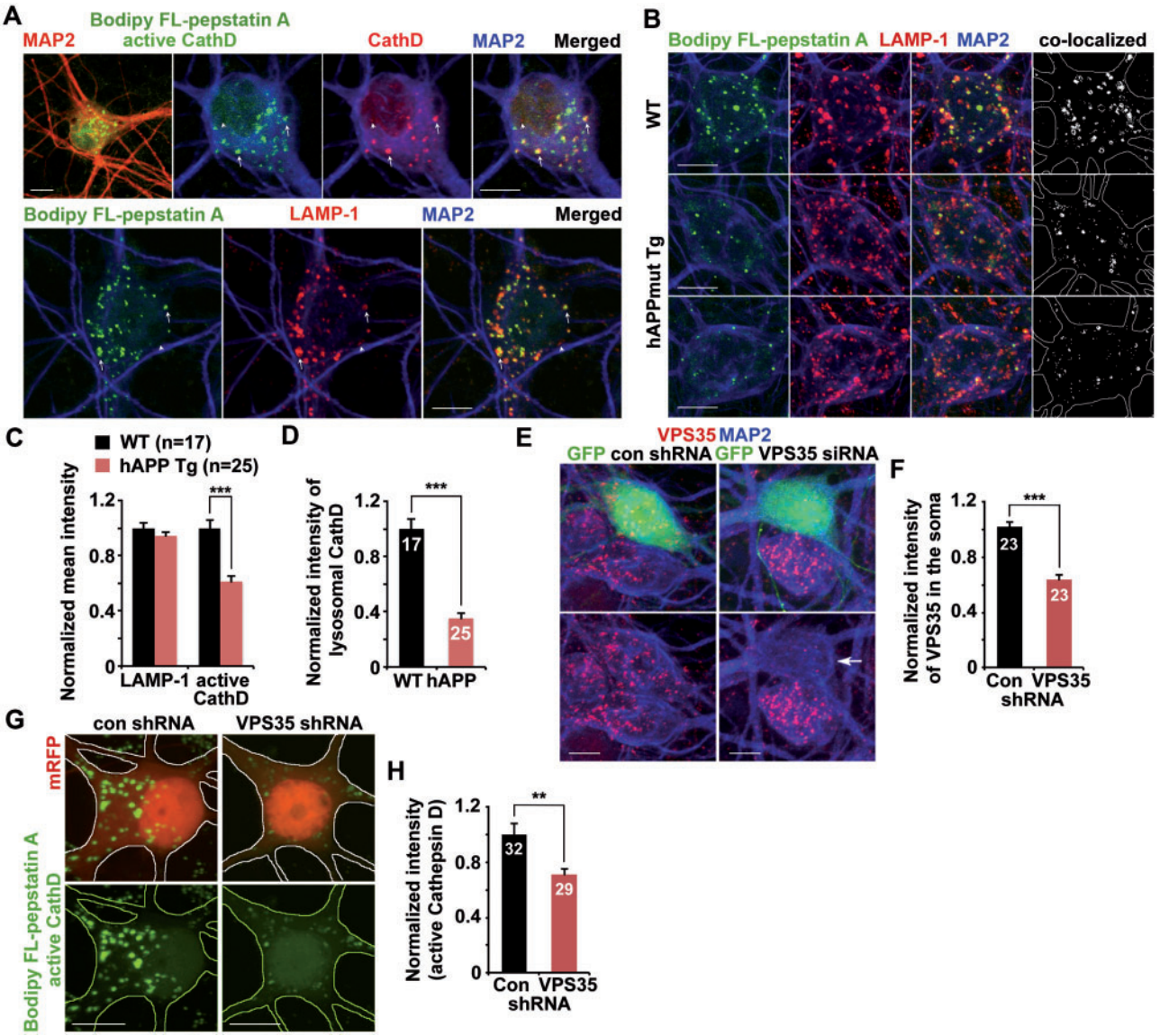

Figure 4. Reduced protease density within lysosomes in mutant hAPP Tg neurons. (**A**) Active protease-loaded mature lysosomes are mainly located in the soma of neurons. The mature form of active Cathepsin D (CathD) was labeled by loading Bodipy FL-pepstatin A for 30 min, followed by fixation and immuostaining with antibodies against Cathepsin D or LAMP-1. Bodipy FL-pepstatin A selectively binds to a mature form of active Cathepsin D within mature acidic lysosomes. The co-labeled organelles reflect mature lysosomes (arrows) while puncta labeled by Cathepsin D or LAMP-1 alone are most likely immature Cathepsin D or immature lysosomes (arrowheads). Note that mature lysosomes labeled by both Bodipy FL-pepstatin A and LAMP-1 are barely detected in MAP2-indicated neuronal processes of cortical neurons. (**B–D**) Representative images (B) and quantitative analysis (C and D) showing reduced density of lysosomal Cathepsin D in cortical neurons from mutant hAPP Tg mice. Data were expressed as the mean intensity of LAMP-1 or active Cathepsin D or the co-localized mean intensity of LAMP-1 with active Cathepsin D, respectively. Note that the density of luminal active Cathepsin D within somatic lysosomes positive for both LAMP-1 and Bodipy FL-pepstatin A was significantly reduced in hAPP neurons. (**E** and **F**) Small hairpin RNA (shRNA)-mediated VPS35 knockdown in WT neurons. Cortical neurons were co-transfected with GFP and VPS35-shRNA or control shRNA at DIV 5, followed by immunostaining with antibodies against VPS35 and MAP2 at DIV10. Arrow points to a neuron with reduced fluorescence intensity of VPS35 in the soma following expressing VPS35-shRNA. The mean intensity of somatic VPS35 was quantified and normalized to that of MAP2 from the same neuron and to those of untransfected neurons from the same imaging fields before comparing to neurons transfected with control shRNA. (**G** and **H**) Reduced intensity of lysosomal active Cathepsin D labeled by Bodipy FL-pepstatin A in the soma of WT neurons expressing VPS35-shRNA. Quantitative data were expressed as normalized mean intensity of Bodipy FL-pepstatin A fluorescence in the soma of VPS35-shRNA expressed neurons relative to that of controls. Scale bars: 10 μm. Data were quantified from a total number of neurons indicated in parentheses (C) or on the top of bars (D, F and H) from at least three independent experiments. Error bars: SEM. Student's *t* test: $^{***}P < 0.001$; $^{**}P < 0.01$.

Attenuation of lysosomal proteolysis deficits through enhanced retromer retrograde transport in mutant hAPP neurons

We previously reported that impaired retrograde transport of late endosomes in AD neurons could be reversed by overexpression of Snapin (26). We next sought to address whether Snapin-enhanced retrograde transport facilitates retromer trafficking toward the soma of AD neurons. Compared to the controls, elevated Snapin expression increased retrograde transport of the retromer protein VPS35 (hAPP: 14.38% ± 1.1%;

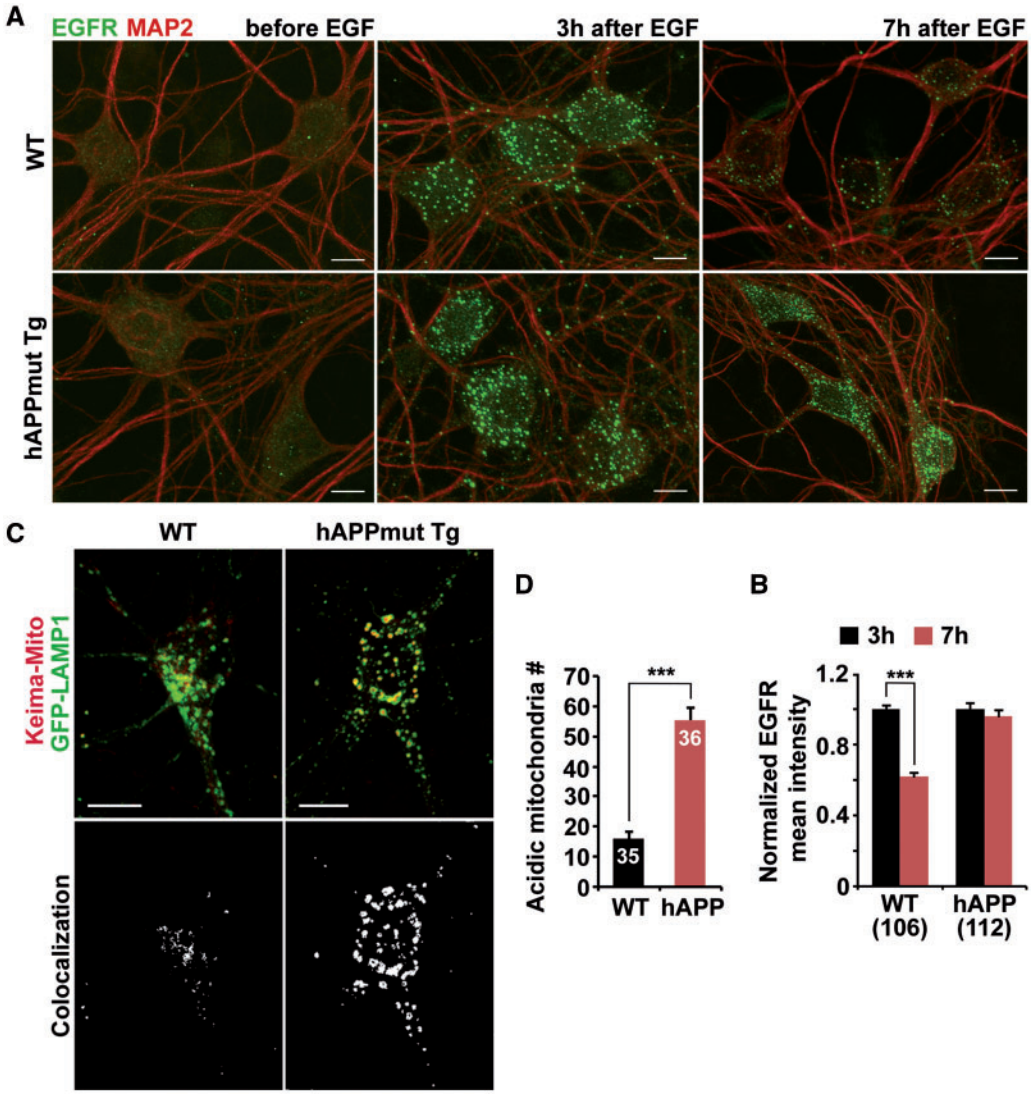

Figure 5. Impaired lysosomal proteolysis in mutant hAPP Tg neurons. (**A** and **B**) Reduced degradation of internalized EGFR in mutant hAPP Tg neurons. Cortical neurons were co-immunostained with EGFR and MAP2 before or 3 or 7 h after EGF incubation (A). The mean intensity of EGFR was normalized against MAP2 from the same neurons and expressed as ratios relative to the mean intensity after 3 h EGF incubation (B). (**C** and **D**) Representative images (C) and quantitative analysis (D) showing aberrant accumulation of acidic mitochondria labeled by Keima-Mito within LAMP-1-marked lysosomal compartments in the soma of mutant hAPP Tg neurons. Visualization of acidic mitochondria is achieved by collecting emission of Keima-Mito at 550 nm. The number of acidic mitochondria within lysosomes per neuron was quantified. Scale bars: 10 μm. Data were quantified from a total number of neurons indicated in parentheses (B) or on the top of bars (D) from at least three independent experiments. Error bars: SEM. Student's *t* test: ***$P < 0.001$.

hAPP with Snapin: 29.89% ± 1.5%; $P < 0.001$) and late endosome-associated VPS35 (hAPP: 15.26% ± 1.54%; hAPP with Snapin: 31.67% ± 2.09%; $P < 0.001$). There were no detectable changes in anterograde transport along the same axon of mutant hAPP Tg neurons (Fig. 7A, B and C). Mutant hAPP neurons expressing Snapin exhibited increased VPS35 density in the soma (VPS35: 1.19 ± 0.03; $P < 0.001$) (Supplementary Material, Fig. S7A and B). Moreover, CI-MPR levels were significantly increased in the soma and in the Golgi of mutant hAPP neurons relative to those of controls (Soma: 1.383 ± 0.076; $P < 0.001$; Golgi: 1.475 ± 0.046; $P < 0.001$) (Supplementary Material, Fig. S7C, D and E). Together, our findings indicate that Snapin-enhanced retrograde transport facilitates the endosome-to-Golgi retrieval of CI-MPR through promoting retromer trafficking to the soma in mutant hAPP neurons.

We further determined whether elevated retromer levels in the soma result in enhanced delivery of proteases, thereby increasing luminal proteases in the somatic lysosome of AD neurons. We found that overexpression of Snapin in hAPP neurons significantly increased the density of Bodipy FL-pepstatin A-labeled active Cathepsin D in the soma (Fig. 7D), as shown to be mainly localized within somatic lysosomes (Fig. 2A). Mutant hAPP neurons in the presence of HA-Snapin displayed ~29% increase in the mean intensity of Bodipy FL-pepstatin A, compared to control hAPP neurons in the absence of HA-Snapin from the same imaging field ($P < 0.001$) (Fig. 7D and E). These data suggest that enhanced retrograde transport of late endosomes facilitates retromer trafficking toward the soma and thus promotes protease transport to lysosomes in AD neurons.

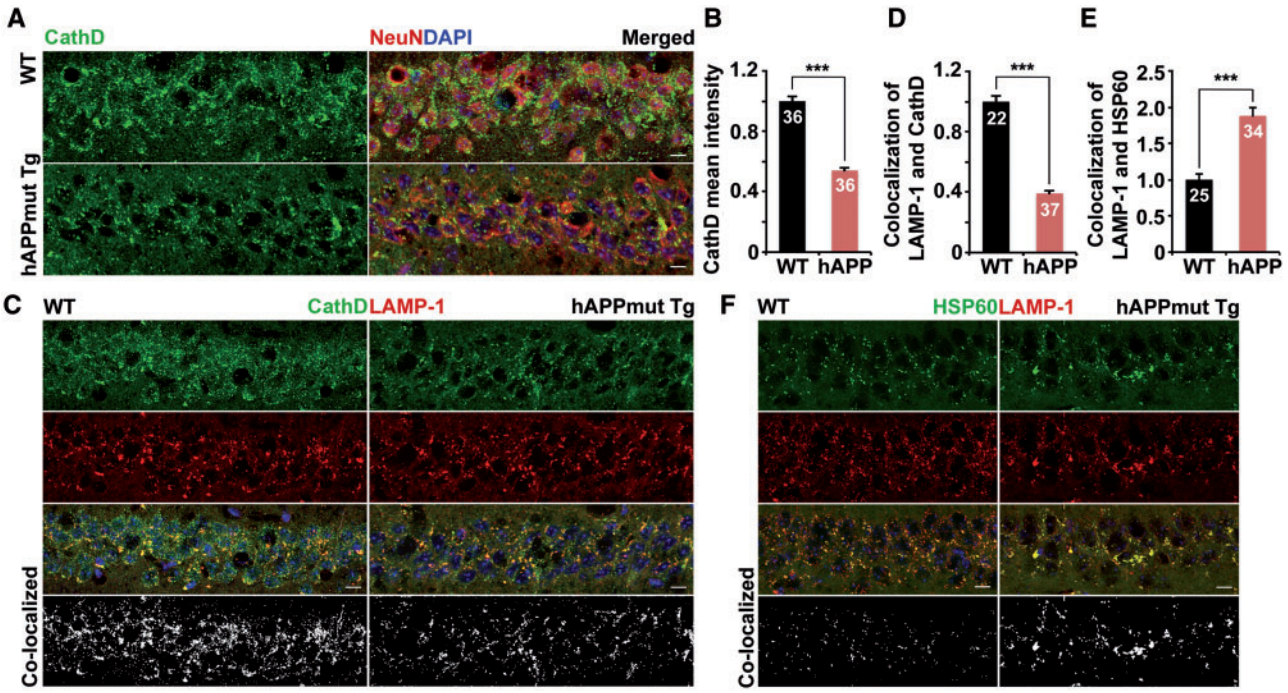

Figure 6. AD-linked lysosomal deficits in mutant hAPP Tg mouse brains. (**A** and **B**) Representative images (A) and quantitative analysis (B) showing reduced density of lysosomal hydrolase Cathepsin D (CathD) in the soma of the hippocampal regions of mutant hAPP Tg mice. Data were expressed as the mean intensity of Cathepsin D per imaging hippocampal slice section (320 μm × 320 μm). (**C** and **D**) Reduced density of lysosomal Cathepsin D in hippocampal neurons of mutant hAPP Tg mice. Note that the co-localized mean intensity of LAMP-1 with CathD is reduced in the soma of the hippocampal regions of mutant hAPP Tg mice. Data were expressed as the co-localized mean intensity of LAMP-1 with Cathepsin D per imaging hippocampal slice section (320 μm × 320 μm). (**E** and **F**) Quantitative analysis (E) and representative images (F) showing aberrant retention of mitochondria within lysosomes in the hippocampal regions of hAPP mice. Data were expressed as co-localized mean intensity of LAMP-1 with HSP60 per imaging hippocampal slice section (320 μm × 320 μm). Scale bars: 10 μm. Data were quantified from a total number of imaging hippocampal slice sections indicated on the top of bars (B, D and E) from three pairs of mice. Error bars: SEM. Student's *t* test: ***$P < 0.001$.

We then tested whether increased levels of lysosomal proteases lead to enhanced lysosomal proteolytic activity in mutant hAPP neurons by providing two lines of evidence. First, elevated Snapin levels resulted in a remarkable reduction in the number of acidic mitochondria within somatic lysosomes in mutant hAPP neurons, suggesting enhanced clearance of defective mitochondria (WT: 11.4 ± 1.57; hAPP: 56.45 ± 4.59; hAPP with Snapin: 14.57 ± 1.43; $P < 0.001$) (Fig. 8A and B). Second, following Snapin overexpression, the density of autolysosomes was markedly decreased in the soma of hAPP neurons (WT: 0.89 ± 0.13; hAPP: 4.51 ± 0.45; hAPP with Snapin: 0.88 ± 0.14; $P < 0.001$) (Fig. 8C and D), which indicates a rescue effect on lysosomal clearance of autophagic cargoes. Altogether, our findings indicate that retrograde transport is critical for trafficking retromer from distal axons toward the soma to fulfil its function in facilitating lysosome biogenesis in the soma, a process that is impaired in AD neurons.

Discussion

Our current study provides new insights into the impact of altered trafficking-induced retromer dysfunction on lysosomal defects in AD neurons: 1) The retromer complex undergoes retrograde transport through its association with late endosomes in the axon of WT neurons, which is impaired in mutant hAPP Tg neurons. Such defects decrease the trafficking of retromer toward the soma (Fig. 1); 2) Retromer is reduced in the soma, but retained within late endosomes in distal axons and at presynaptic terminals in the brains of mutant hAPP mice and human AD patients (Fig. 2 and Supplementary Material, Fig. S4); 3) Mutant hAPP neurons show retromer dysfunction in the soma, as evidenced by the impairment of retromer-mediated Golgi targeting of CI-MPR (Fig. 3); 4) Luminal proteases in the lysosome are decreased in the soma of mutant hAPP neurons and mouse brains, leading to defective lysosomal degradation of internalized EGFR and defective mitochondria (Figs 4–6); 5) Enhanced retrograde axonal transport of late endosomes facilitates retromer trafficking toward the soma, thereby rescuing lysosomal proteolysis deficits in AD neurons (Figs 7 and 8). Our study reveals, for the first time, that AD-linked lysosomal deficits are attributed to retromer dysfunction due to its altered trafficking in the axon. Given the fact that CI-MPR-dependent protease transport to the lysosome mainly occurs in the soma, enhanced retrograde transport facilitates retromer to fulfil its role in the soma in mediating the retrieval of CI-MPR from the late endosome to the Golgi, a crucial step required for lysosomal biogenesis. Our study sets the stage for future investigations into genetic and pharmacological dissection of factors that influence lysosomal proteolytic activity through the regulation of retromer trafficking in AD.

Retromer deficiency has been linked to AD, contributing to the core pathological features of the disease. However, the pathogenic link between retromer and AD has yet to be established (11). We demonstrate that retromer associates with late endosomes enriched in the axon of neurons (Fig. 1). A significant portion of retromer co-localizes and co-migrates with late endosomes in a retrograde direction along the axon toward the soma. There, it traffics endosomal CI-MPR to the Golgi, which is required for lysosome biogenesis. However, in mutant hAPP neurons, retrograde transport of retromer is impaired, leading

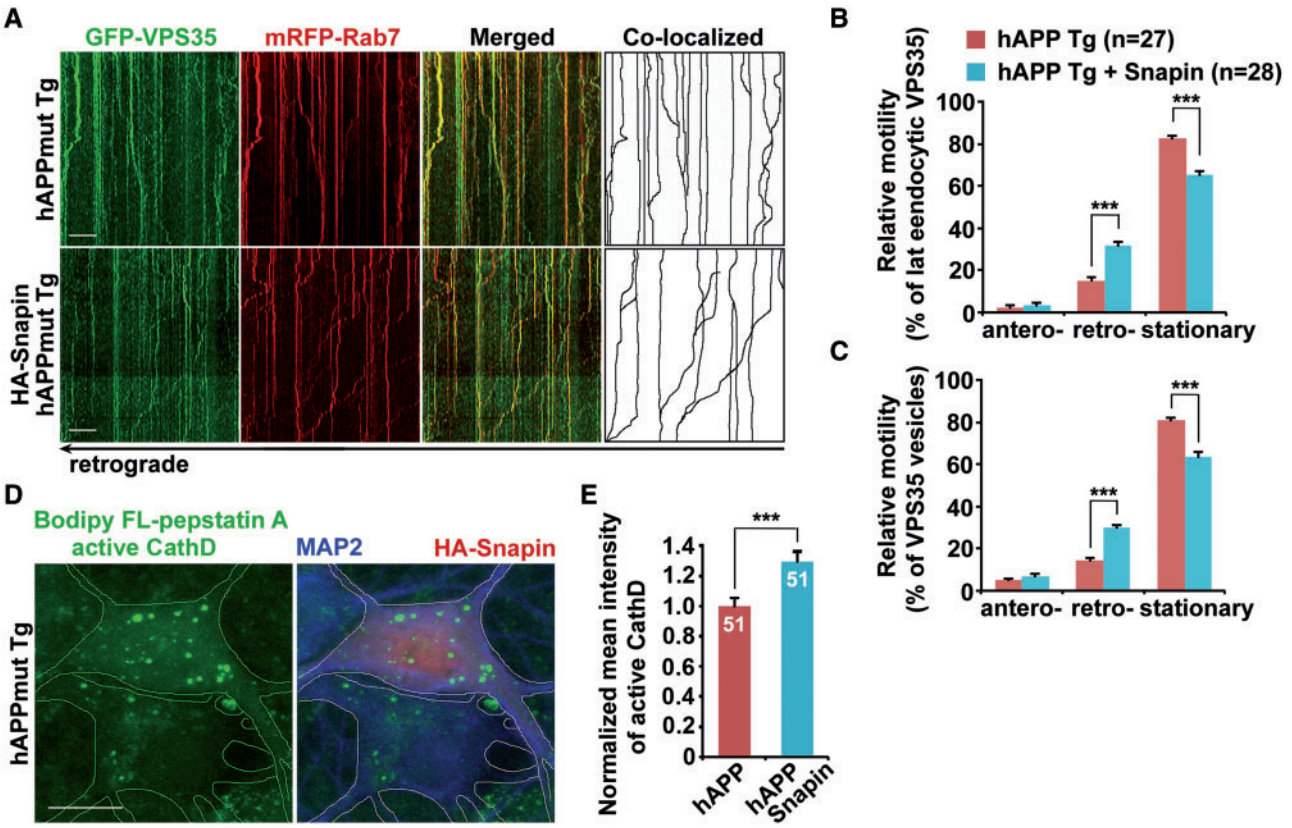

Figure 7. Increasing lysosomal delivery of proteases through enhanced retrograde transport of axonal retromer in mutant hAPP Tg neurons. (**A–C**) Representative kymographs (A) and quantitative analysis (B and C) showing enhanced retrograde transport of late endosomal retromer following overexpression of Snapin in mutant hAPP Tg neurons. (**D** and **E**) Increased density of active Cathepsin D (CathD) labeled by Bodipy FL-pepstatin A in the soma of hAPP neurons expressing Snapin. The mean intensities of Bodipy FL-pepstatin A in the soma of hAPP neurons in the presence and absence of Snapin from the same imaging fields were quantified. Scale bars: 10 μm. Data were quantified from a total number of neurons indicated in parentheses (B and C) or on the top of bars (E) from at least three independent experiments. Error bars represent SEM. Student's *t* test: $^{***}p < 0.001$.

to its abnormal retention in distal axons and thus a significant reduction in the soma (Figs 1 and 2). As a result, somatic retromer deficiency impairs lysosomal delivery of proteases via CI-MPR (Figs 3 and 4). Conversely, enhanced retrograde transport in AD neurons rescues somatic retromer deficiency by facilitating retromer trafficking toward the soma, thereby correcting lysosomal proteolysis deficits (Figs 7 and 8). Therefore, our data indicate a possible link between altered trafficking-induced retromer dysfunction and lysosomal defects in AD, linking to the mechanism of AD pathogenesis.

Reduced levels in the retromer proteins VPS35 and VPS26 were reported in certain disease-affected areas of human AD patient brains, particularly in the entorhinal cortex, but not in the dentate gyrus (17). In our study, we examined the hippocampal regions from AD patient brains. We found that while VPS35 accumulated in presynaptic terminals of the hippocampus, it exhibited no significant reduction in the post-nuclear supernatants relative to that of control subjects (0.77 ± 0.14; P = 0.166) (Supplementary Material, Fig. S4). Thus, our data are consistent with those of previous studies (17). In the current study, mutant hAPP Tg (J20) mouse brains and cultured neurons also do not exhibit any detectable reduction in the levels of the core retromer protein VPS35 (Supplementary Material, Fig. S2), which excludes the possibility of global retromer deficiency. Moreover, we found that AD patient brains show abnormal retention of retromer at presynaptic terminals (Supplementary Material, Fig. S4), a phenotype similar to that of mutant hAPP Tg mice (Figs 1 and 2). Such defects lead to retromer dysfunction in the soma, thereby resulting in impaired lysosome biogenesis and defective lysosomal proteolysis in AD neurons. Pharmacological chaperones aiming to stabilize the retromer complex have been investigated to rescue retromer deficiency in AD (38). Our findings allow us to propose a new strategy to enhance retromer functionality in AD neurons by increasing retrograde axonal transport of retromer.

The trafficking mechanism of the retromer has been studied mostly in many non-neuronal cell types. It remains unknown how retromer trafficking is regulated in neurons. Retromer was reported to support AMPA receptor trafficking during dendritic spine maturation and LTP (12,13,32,33). Moreover, the retromer complex was shown to associate with dynein/dynactin motor complex (39,40), and regulate retrograde axonal trafficking of BACE1 (18,41). In the axon of WT neurons, we consistently found that a significant portion of retromer co-localizes and co-migrates with late endosomes in a retrograde direction (Fig. 1). However, retromer in the dendrite exhibits a short-range bidirectional trafficking pattern and associates much less with late endosomes (Supplementary Material, Fig. S1). Thus, our results indicate a differential mechanism regulating axonal versus dendritic retromer trafficking. We propose that dendritic retromer may play a major role in regulating local trafficking events, whereas axonal retromer undergoes long-distance retrograde transport to fulfill its function in the soma of neurons.

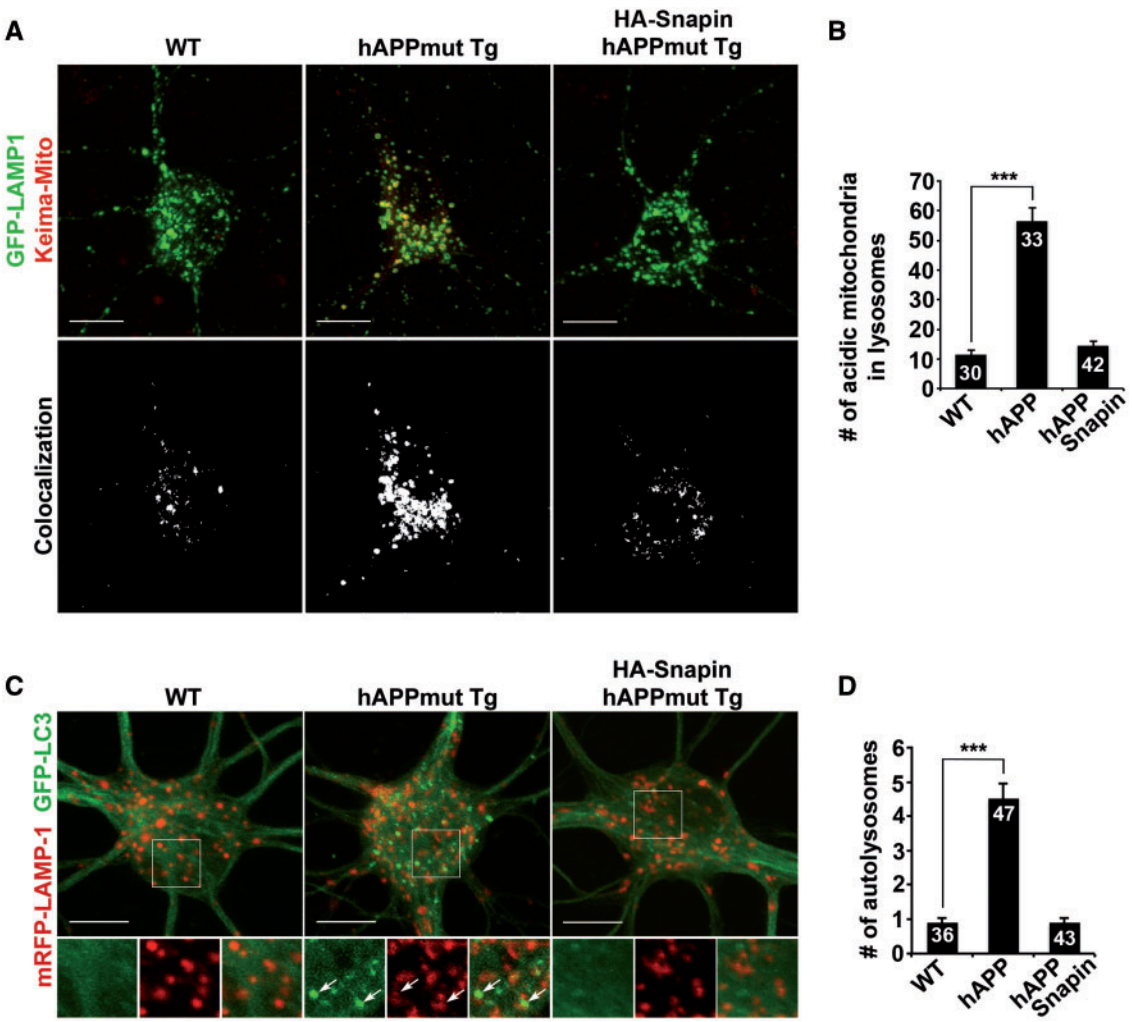

Figure 8. Enhanced retrograde transport-resulted attenuation of lysosomal proteolysis deficits in mutant hAPP neurons. (**A** and **B**) Snapin-enhanced retrograde transport reduces accumulation of acidic mitochondria within lysosomes in the soma of hAPP neurons. The average number of acidic mitochondria within lysosomes in the soma of neurons was quantified. (**C** and **D**) Representative images (C) and quantitative analysis (D) showing that elevated Snapin expression facilitates lysosomal clearance of autophagic cargoes in hAPP neurons. Note that autolysosomes were accumulated in hAPP neurons, but were markedly reduced following overexpression of Snapin. The average number of autolysosomes co-labeled by GFP-LC3 and mRFP-LAMP-1 in the soma of neurons was quantified. Scale bars: 10 μm. Data were quantified from a total number of neurons (n) as indicated on the top of the bar (B and D) from at least four independent repeats. Error bars: SEM. Student's *t* test: ***$P < 0.001$.

In our recent study, we provided mechanistic insights into defects in the retrograde transport of late endosomes/amphisomes in AD neurons (34,42). We demonstrated that direct interaction of oligomeric Aβ1-42 with dynein intermediate chain (DIC) disrupts the coupling of dynein-Snapin, a motor-adaptor complex essential for recruiting dynein transport machinery to late endosomes. As a result, this interaction impairs the recruitment of dynein motors to late endosomes, thereby immobilizing them in distal axons. Taken together, we proposed that such defects likely result in impaired retromer trafficking to the soma for the fulfillment of its function in AD neurons.

Lysosomal dysfunction is a prominent feature in AD brains, and has been linked to AD pathogenesis. Inhibiting lysosomal proteolysis produces similar neuropathology in WT mice and also exacerbates amyloid and autophagy pathology in mouse models of AD (28,43). Proteins and key genetic risk factors such as presenillin 1 mutations and ApoE4, which are known to be involved in AD pathogenesis, directly impair lysosomal function (44). Other factors contributing to AD pathogenesis, which include reactive oxygen species (ROS), Aβ peptides, and oxidized lipids and lipoproteins, similarly impede lysosomal proteolysis, leading to apoptosis and neuronal cell death due to toxic accumulation, as seen in the disease (44). In the current study, we propose that impaired targeting of proteases to the lysosome leads to defects in lysosomal proteolysis in AD neurons. Proper delivery of newly synthesized proteases from the TGN to the endo-lysosomal system depends on the presence of CI-MPR at the Golgi. Retromer facilitates this process by mediating the retrieval of CI-MPR from the late endosome to the TGN (11). Our results indicate that impaired transport of proteases to the lysosome in AD neurons is attributed to defective CI-MPR recycling to the Golgi as a result of retromer dysfunction in the soma (Figs 2–4 and 6). Thus, protease deficiency in lysosomes disrupts lysosomal proteolytic activity, backing up damaged mitochondria and autophagic cargoes in swollen lysosomes or autolysosomes in AD neurons (Figs 5 and 8).

Mounting evidence demonstrated that autophagosomes are robustly generated in distal axons and move continuously in a retrograde direction toward the soma, where major clearance of autophagic cargoes occurs following fusion with somatic

lysosomes (45–47). Moreover, in order to gain long-distance retrograde motility, newly generated autophagosomes inevitably fuse with late endosomes to form amphisomes for their recruitment of dynein motor transport machinery (46). A recent study reported that lysosomes deficient in luminal proteases are accumulated in the axon of an AD mouse model (37). Such defects were proposed to impair autolysosomal proteolysis for eliminating autophagic substrates from autolysosomes in the axon and thus contribute to massive accumulation of such autolysosomes. However, this study did not exclude the possibility that the accumulated organelles in the axon may represent amphisomes rather than lysosomes or autolysosomes, since they all are positive for LAMP-1. In accordance with this view, several studies have shown that autophagic organelles, in particular amphisomes, are massively accumulated in dystrophic axons of AD brains (4,34,37,48).

It has been shown that active proteases are preferentially enriched in the somatic lysosome of neurons (27,28,31,37). Consistently, we demonstrated that lysosomes enriched with active proteases are concentrated in the soma of WT neurons (Fig. 4). However, lysosomal proteases are markedly reduced in AD neurons, leading to defects in the clearance of sequestered substrates within the lysosome (Figs 4–6). Our data is consistent with previous studies showing impaired lysosomal Cathepsin activities in the soma of neurons from another mouse model of AD (49). In the current study, we further reveal that enhancing retrograde transport of the retromer complex corrects deficits in the elimination of lysosomal substrates by increasing luminal proteases levels in the lysosome (Figs 7 and 8). Autophagic clearance has been shown to primarily take place in the soma of neurons (31,45,46). Impaired retrograde transport was proposed to contribute to autophagic stress in the distal axon of AD brains (34,37). Thus, in our study, enhanced retrograde transport may also facilitate targeting axonal autophagic cargoes for lysosomal clearance in the soma of AD neurons.

In conclusion, the current study advances our understanding of lysosomal defects in AD brains, and provides new cellular insights into the complex regulation of neuronal lysosome biogenesis by coordinating retrograde transport of retromer in the axon and retromer-mediated CI-MPR recycling to the Golgi in the soma, as well as how defects in this cellular pathway lead to impaired lysosomal proteolysis and substrate accumulation in AD neurons. Our data also allows us to propose a model that enhanced retrograde trafficking of retromer in the axon facilitates lysosome biogenesis in the soma. Further therapeutic approaches aimed at modulating retrograde axonal transport of retromer may help rescue lysosomal proteolysis deficits associated with AD. Given that AD neurons display unaltered Snapin levels (Supplementary Material, Fig. S2), up-regulation of Snapin-mediated mechanism could serve as a therapeutic strategy to treat AD-linked lysosomal deficits. The study may have a broader relevance to other neurodegenerative diseases with retromer deficiency and a lysosomal component to their pathology.

Materials and Methods

Mice

hAPP mice (C57BL/6J) from line J20 (https://www.jax.org/strain/006293) (30) were purchased from the Jackson Laboratory.

Human brain specimens

Five postmortem brain specimens from AD patients diagnosed with AD according to Braak criteria (50) and four age-matched control subjects were obtained from the Harvard Tissue Resource Center and the Human Brain and Spinal Fluid Resource Center at UCLA. The specimens were from hippocampus and were both quick-frozen (BA9).

Materials

Sources of antibodies or reagents are as follows: polyclonal antibodies against Cathepsin D (Cat# AF1029, RRID: AB_2087094) (R&D systems), HSP60 (Cat# 4870S, RRID: AB_2295614) (Cell Signaling Technology), EEA1 (Cat# sc-6416, RRID: AB_640035) and MAP2 (Cat# sc-20172, RRID: AB_2250101) (Santa Cruz), Cathepsin B (Cat# AF965, RRID: AB_2665929), Cathepsin L (Cat# AF1515, RRID: AB_2665930), and VPS35 (Cat# NB100-1397, RRID: AB_527526) (Novus), CI-MPR (Cat# ab124767, RRID: AB_10974087) (Abcam); monoclonal antibodies against LAMP-1 (Cat# 1d4b, RRID: AB_2134500) (Developmental Studies Hybridoma Bank), Neu N (Cat# MAB377, RRID: AB_2298772), DIC (Cat# MAB1618, RRID: AB_2246059), GAPDH (Cat# CB1001, RRID: AB_2107426), and synaptophysin (Cat# MAB5258, RRID: AB_11214133) (Millipore), MAP2 (Cat# 556320, RRID: AB_396359) (BD pharmingen), GM130 (Cat# 610822, RRID: AB_398141) and EGFR (Cat# 610017, RRID: AB_2096701) (BD transduction), synaptophysin (Cat# sc-9116, RRID: AB_2199007) and VPS35 (Cat# 374372, RRID: AB_10988942) (Santa Cruz), VPS26 (Cat# ab181352, RRID: AB_2665924) (Abcam), Rab7 (Cat# R8779, RRID: AB_609910) (Sigma); HA (Cat# 901501, RRID: AB_2565006) (Biolegend); Transferrin receptor (Cat# 13-6800, RRID: AB_2533029), and Alexa fluor 488- (Cat# A11070, RRID: AB_142134) (Cat# A11017, RRID: AB_2534115) (Cat# A11055, RRID: AB_2534102), 546- (Cat# A11071, RRID: AB_2534115) (Cat# A11018, RRID: AB_2534085), and 633- (A21072, RRID: AB_2535733) (Cat# A21053, RRID: AB_2535720) conjugated secondary antibodies (Invitrogen); Bodipy FL-pepstatin A (Cat# P12271) (Invitrogen); Magic Red (Cat# 937) (ImmunoChemistry Technologies); control (Cat# sc-108060) and VPS35 shRNA (Cat# sc-63219) (Santa Cruz).

Transfection and immunocytochemistry of cultured cortical neurons

Cortices were dissected from E18-19 mouse embryos as described (27,51,52). Cortical neurons were dissociated by papain (Worthington) and plated at a density of 100, 000 cells per cm^2 on polyornithine- and fibronectin-coated coverslips. Neurons were grown overnight in plating medium (5% FBS, insulin, glutamate, G5 and 1 × B27) supplemented with 100 × L-glutamine in Neurobasal medium (Invitrogen). Starting at DIV 2, cultures were maintained in conditioned medium with half-feed changes of neuronal feed (1 × B27 in Neurobasal medium) every 3 days. Primary hAPP Tg neurons were cultured from breeding mice of hemizygous mutant hAPPSwe/Ind Tg (J20 line) with WT animals (30). Genotyping assays were performed following culture plating to verify mouse genotypes. In our study, we examined both transgenic neurons and non-transgenic neurons derived from their littermates. WT and mutant hAPP Tg neurons were transfected with various constructs at DIV6-8 using Lipofectamine 2000 (Invitrogen), followed by time-lapse imaging 7–13 days after transfection and prior to quantification analysis.

For immunostaining, cultured neurons were fixed with 4% formaldehyde (Polyscience, Inc.) and 4% sucrose (Sigma) in 1 ×

phosphate-buffered saline (PBS) at room temperature (RT) for 20 min, or 100% ice-cold methanol at -20 °C for 10 min, washed three times with PBS for 5 min each, and then incubated in 0.4% saponin, 5% normal goat serum (NGS) and 2% bovine serum albumin (BSA) in PBS for 1 h. Fixed cultures were incubated with primary antibodies in PBS with 2% BSA and 0.4% saponin at 4 °C overnight. Cells were washed four times with PBS at RT for 5 min each, incubated with secondary fluorescent antibodies at 1:400 dilution in PBS with 2% BSA and 0.4% saponin for 30 min, re-washed with PBS, and then mounted with Fluor-Gel antifade mounting medium (EMS) for imaging.

For labeling active Cathepsin D by Bodipy FL-pepstatin A, live neurons were incubated with 1 μM Bodipy-FL-pepstatin A in Neurobasal medium for 1 h at 37 °C, followed by fixation and immunostaining with antibodies against MAP2 and LAMP-1.

For labeling active Cathepsin B by the cresyl violet fluorogenic substrate CV-(Arg-Arg)2 (Magic Red), live neurons were incubated with staining solution (MR-RR2) at 1:500 dilution for 15 min at 37 °C, then washed three times by Neurobasal medium for imaging.

For EGFR degradation assay, cortical neurons were starved in culture medium in the absence of B27 supplement for 15 min and then treated for 30 min at 4 °C with culture medium containing EGF (5 μg/ml), followed by incubation at 37 °C with medium in the absence of EGF for various times before fixation and immunostaining with antibodies against MAP2 and EGFR.

Image acquisition and quantification

Confocal images were obtained using an Olympus FV1000 oil immersion 60× objective (1.3 numerical aperture) with a sequential-acquisition setting. For fluorescent quantification, images were acquired using the same settings below saturation at a resolution of 1024 ×1024 pixels (8 bit). Eight to ten sections were taken from the top-to-bottom of the specimen and brightest point projections were made. Morphometric measurements were performed using NIH ImageJ. Measured data were imported into Excel software for analysis. The thresholds in all images were set to similar levels. Fluorescence intensity of LAMP-1, Bodipy FL-pepstatin A, or VPS35 was expressed in arbitrary units of fluorescence per square area. The mean intensity of LAMP-1, Bodipy FL-pepstatin A or VPS35 in the soma of mutant hAPP Tg cortical neurons was normalized as a percentile ratio relative to that in WT control neurons. Data was obtained from at least three independent experiments and the number of neurons used for quantification is indicated in the figures. All statistical analyses were performed using the Student's *t*-test and are presented as mean ± SEM.

Criteria for axon selection in cultured neurons

For analyzing mitochondrial motility in live neurons, we selected axons for time-lapse imaging and measuring mitochondrial motility because axons, but not dendrites, have uniform microtubule organization and polarity. Axonal processes were selected as we previously reported (26,27,51). Briefly, axons in live images were distinguished from dendrites based on known morphologic characteristics: greater length, thin and uniform diameter, and sparse branching (53). Only those that appeared to be single axons and separate from other processes in the field were chosen for recording axonal mitochondrial transport. Regions where crossing or fasciculation occurred were excluded from analysis.

For live cell time-lapse imaging, neurons were transferred to Tyrode's solution containing 10 mM Hepes, 10 mM glucose, 1.2 mM $CaCl_2$, 1.2 mM $MgCl_2$, 3 mM KCl and 145 mM NaCl, pH 7.4. Temperature was maintained at 37 °C with an air stream incubator. Cells were visualized with a 60× oil immersion lens (1.3 numerical aperture) on an Olympus FV1000 confocal microscope, using 458 excitation for CFP, 488 nm for GFP or YFP, and 559 nm for DsRed. Time-lapse sequences of 1024 ×1024 pixels (8 bit) were collected at 5-s intervals with 1% intensity of the laser to minimize laser-induced bleaching and cell damage while maximizing pinhole opening. Time-lapse images were captured at a total of 100 frames. Recordings were started 6 min after the coverslip was placed in the chamber. The stacks of representative images were imported into NIH ImageJ software and converted to QuickTime movies. A vesicle or membranous organelle was considered stopped if it remained stationary for the entire recording period; a motile one was counted only if it displaced at least 5 μm. To trace axonal anterograde or retrograde movement of vesicles or organelles and to count stationary ones, kymographs were made as described previously (51,54) with extra plug-ins for ImageJ (NIH). Briefly, we used the 'Straighten' plugin to straighten curved axons, and the 'Grouped ZProjector' to z-axially project re-sliced time-lapse images. The height of the kymographs represents recording time (300 s unless otherwise noted), while the width represents the length (μm) of the axon imaged. Counts were averaged from 100 frames for each time-lapse image to ensure accuracy of stationary and motile events. Relative motility of vesicles or organelles is described as the percentage of anterograde, retrograde, or stationary events of total vesicles or organelles. Measurements are presented as mean ± SEM. Statistical analyses were performed using unpaired Student's *t*-tests.

Tissue preparation and immunohistochemistry

Animals were anaesthetized with 2.5% avertin (0.5 ml per mouse) and transcardially perfused with fixation buffer (4% paraformaldehyde in PBS, pH 7.4). Brains were dissected out and post fixed in fixation buffer overnight and then placed in 30% sucrose at 4 °C. 10-μm-thick coronal sections were collected consecutively to the level of the hippocampus and used to study co-localization of various markers. After incubation with blocking buffer (2.5% goat serum, 0.15% Triton X-100, 1.5% BSA, 0.5% glycine in H_2O) at RT for 1 h, the sections were incubated with primary antibodies at 4 °C overnight, followed by incubation with secondary fluorescence antibodies at 1:600 dilution at RT for 1 h. After fluorescence immuno-labeling, the sections were stained with DAPI and washed three times in PBS. The sections were then mounted with anti-fading medium (vector laboratories, H-5000) for imaging.

Immunoisolation of late endocytic organelles

Brain tissues from WT mice were homogenized in the buffer (10 mM HEPES [pH 7.4], 1 mM EDTA, 0.25 M sucrose and protease inhibitors) and centrifuged at 800*g* for 10 min, and then the supernatant was collected. The pellet was re-suspended in the homogenization buffer using a glass rod with 3–4 gentle strokes of the pestle of the 30-ml Dounce Homogenizer and re-centrifuged at 800*g* for 10 min. The combined first and second supernatants were centrifuged at 3500*g* for 10 min and then collected for high-speed centrifugation at 20 000*g* for 10 min. The pellet was re-suspended in the homogenization buffer using a glass rod

with 3 to 4 gentle strokes of the pestle of the 30-ml Dounce Homogenizer and re-centrifuged at 20 000*g* for 10 min. The pellet was then re-suspended in the homogenization buffer and subjected to immuno-isolation with tosylated linker-coated superparamagnetic beads (Dynabeads M-450 Subcellular; Invitrogen) as described in previous studies (26,27,46,55). For all subsequent steps, beads were collected with a magnetic device (MPC; Invitrogen). After washing once for 5 min in PBS (pH 7.4) with 0.1% BSA at 4 °C, the linker-coated beads (1.4 mg) were incubated with 1 μg anti-Rab7 mAb, or control mouse IgG overnight at 4 °C on a rotator. After incubation, the beads were washed four times (5 min each) in PBS [pH 7.4] with 0.1% BSA at 4 °C, and then re-suspended in an incubation buffer containing PBS [pH 7.4], 2 mM EDTA, and 5% fetal bovine serum. Approximately 400 μg of light membrane fraction from WT mouse brains were mixed with incubation buffer containing beads (final reaction volume 1 ml) and incubated for 4 h at 4 °C on a rotator. After incubation, the beads were collected with a magnetic device and washed five times with the incubation buffer and three times with PBS for 10 min each and then resolved by 4–12% Bis-Tris PAGE for sequential Western blots on the same membranes after stripping between each application of the antibody.

Supplementary Material

Supplementary Material is available at *HMG* online.

Acknowledgements

We thank Z-H. Sheng for GFP-LAMP-1 and Keima-Mito plasmids and Snapin antibody; P. Cullen for GFP-VPS35; A. Helenius for mRFP-Rab7; D. Sabatini for LAMP-1-mRFP; E Gavin, X Su, C Agrawal, J Cheung, P Tiwari, and other members in Q.C lab for their research assistance; Harvard Tissue Resource Center supported by National Institutes of Health grant HHSN-271-2013-00030C and Human Brain and Spinal Fluid Resource Center at UCLA for providing the postmortem brain specimens from AD patients and age-matched control subjects. This research was supported by National Institutes of Health grants R00AG033658, R01NS089737 and R21NS102780.

Conflict of Interest statement. None declared.

References

1. Luzio, J.P., Pryor, P.R. and Bright, N.A. (2007) Lysosomes: fusion and function. *Nat. Rev. Mol. Cell. Biol.*, **8**, 622–632.
2. Saftig, P. and Klumperman, J. (2009) Lysosome biogenesis and lysosomal membrane proteins: trafficking meets function. *Nat. Rev. Mol. Cell. Biol.*, **10**, 623–635.
3. Saftig, P. and Haas, A. (2016) Turn up the lysosome. *Nat. Cell. Biol.*, **18**, 1025–1027.
4. Nixon, R.A. (2005) Endosome function and dysfunction in Alzheimer's disease and other neurodegenerative diseases. *Neurobiol. Aging*, **26**, 373–382.
5. Nixon, R.A. and Cataldo, A.M. (2006) Lysosomal system pathways: genes to neurodegeneration in Alzheimer's disease. *J. Alzheimers Dis.*, **9**, 277–289.
6. Seaman, M.N. (2004) Cargo-selective endosomal sorting for retrieval to the Golgi requires retromer. *J. Cell. Biol.*, **165**, 111–122.
7. Sullivan, C.P., Jay, A.G., Stack, E.C., Pakaluk, M., Wadlinger, E., Fine, R.E., Wells, J.M. and Morin, P.J. (2011) Retromer disruption promotes amyloidogenic APP processing. *Neurobiol. Dis.*, **43**, 338–345.
8. Burd, C. and Cullen, P.J. (2014) Retromer: a master conductor of endosome sorting. *Cold Spring Harb. Perspect. Biol.*, **6**, a016774.
9. Hierro, A., Rojas, A.L., Rojas, R., Murthy, N., Effantin, G., Kajava, A.V., Steven, A.C., Bonifacino, J.S. and Hurley, J.H. (2007) Functional architecture of the retromer cargo-recognition complex. *Nature*, **449**, 1063–1067.
10. Arighi, C.N., Hartnell, L.M., Aguilar, R.C., Haft, C.R. and Bonifacino, J.S. (2004) Role of the mammalian retromer in sorting of the cation-independent mannose 6-phosphate receptor. *J. Cell. Biol.*, **165**, 123–133.
11. Small, S.A. and Petsko, G.A. (2015) Retromer in Alzheimer disease, Parkinson disease and other neurological disorders. *Nat. Rev. Neurosci.*, **16**, 126–132.
12. Tian, Y., Tang, F.L., Sun, X., Wen, L., Mei, L., Tang, B.S. and Xiong, W.C. (2015) VPS35-deficiency results in an impaired AMPA receptor trafficking and decreased dendritic spine maturation. *Mol. Brain*, **8**, 70.
13. Temkin, P., Morishita, W., Goswami, D., Arendt, K., Chen, L. and Malenka, R. (2017) The retromer supports AMPA receptor trafficking during LTP. *Neuron*, **94**, 74–82 e75.
14. Tang, F.L., Liu, W., Hu, J.X., Erion, J.R., Ye, J., Mei, L. and Xiong, W.C. (2015) VPS35 deficiency or mutation causes dopaminergic neuronal loss by impairing mitochondrial fusion and function. *Cell Rep.*, **12**, 1631–1643.
15. Wang, W., Wang, X., Fujioka, H., Hoppel, C., Whone, A.L., Caldwell, M.A., Cullen, P.J., Liu, J. and Zhu, X. (2015) Parkinson's disease-associated mutant VPS35 causes mitochondrial dysfunction by recycling DLP1 complexes. *Nat. Med.*, **22**, 54–63.
16. Wang, W., Ma, X., Zhou, L., Liu, J. and Zhu, X. (2017) A conserved retromer sorting motif is essential for mitochondrial DLP1 recycling by VPS35 in Parkinson's disease model. *Hum. Mol. Genet.*, **26**, 781–789.
17. Small, S.A., Kent, K., Pierce, A., Leung, C., Kang, M.S., Okada, H., Honig, L., Vonsattel, J.P. and Kim, T.W. (2005) Model-guided microarray implicates the retromer complex in Alzheimer's disease. *Ann. Neurol.*, **58**, 909–919.
18. Wen, L., Tang, F.L., Hong, Y., Luo, S.W., Wang, C.L., He, W., Shen, C., Jung, J.U., Xiong, F., Lee, D.H. *et al.* (2011) VPS35 haploinsufficiency increases Alzheimer's disease neuropathology. *J. Cell. Biol.*, **195**, 765–779.
19. Muhammad, A., Flores, I., Zhang, H., Yu, R., Staniszewski, A., Planel, E., Herman, M., Ho, L., Kreber, R., Honig, L.S. *et al.* (2008) Retromer deficiency observed in Alzheimer's disease causes hippocampal dysfunction, neurodegeneration, and Abeta accumulation. *Proc. Natl. Acad. Sci. USA*, **105**, 7327–7332.
20. Kang, H., Kim, S.Y., Song, K., Sohn, E.J., Lee, Y., Lee, D.W., Hara-Nishimura, I. and Hwang, I. (2012) Trafficking of vacuolar proteins: the crucial role of Arabidopsis vacuolar protein sorting 29 in recycling vacuolar sorting receptor. *Plant Cell*, **24**, 5058–5073.
21. Priya, A., Kalaidzidis, I.V., Kalaidzidis, Y., Lambright, D. and Datta, S. (2015) Molecular insights into Rab7-mediated endosomal recruitment of core retromer: deciphering the role of Vps26 and Vps35. *Traffic*, **16**, 68–84.
22. Seaman, M.N., Harbour, M.E., Tattersall, D., Read, E. and Bright, N. (2009) Membrane recruitment of the cargo-selective retromer subcomplex is catalysed by the small GTPase Rab7 and inhibited by the Rab-GAP TBC1D5. *J. Cell. Sci.*, **122**, 2371–2382.
23. Nakada-Tsukui, K., Saito-Nakano, Y., Ali, V. and Nozaki, T. (2005) A retromerlike complex is a novel Rab7 effector that is involved in the transport of the virulence factor cysteine

protease in the enteric protozoan parasite Entamoeba histolytica. *Mol. Biol. Cell.*, **16**, 5294–5303.
24. Bonifacino, J.S. and Hurley, J.H. (2008) Retromer. *Curr. Opin. Cell Biol.*, **20**, 427–436.
25. Sangare, L.O., Alayi, T.D., Westermann, B., Hovasse, A., Sindikubwabo, F., Callebaut, I., Werkmeister, E., Lafont, F., Slomianny, C., Hakimi, M.A. *et al.* (2016) Unconventional endosome-like compartment and retromer complex in Toxoplasma gondii govern parasite integrity and host infection. *Nat. Commun.*, **7**, 11191.
26. Ye, X. and Cai, Q. (2014) Snapin-mediated BACE1 retrograde transport is essential for its degradation in lysosomes and regulation of APP processing in neurons. *Cell Rep.*, **6**, 24–31.
27. Cai, Q., Lu, L., Tian, J.H., Zhu, Y.B., Qiao, H. and Sheng, Z.H. (2010) Snapin-regulated late endosomal transport is critical for efficient autophagy-lysosomal function in neurons. *Neuron*, **68**, 73–86.
28. Lee, S., Sato, Y. and Nixon, R.A. (2011) Lysosomal proteolysis inhibition selectively disrupts axonal transport of degradative organelles and causes an Alzheimer's-like axonal dystrophy. *J. Neurosci.*, **31**, 7817–7830.
29. Braulke, T. and Bonifacino, J.S. (2009) Sorting of lysosomal proteins. *Biochim. Biophys. Acta*, **1793**, 605–614.
30. Mucke, L., Masliah, E., Yu, G.Q., Mallory, M., Rockenstein, E.M., Tatsuno, G., Hu, K., Kholodenko, D., Johnson-Wood, K. and McConlogue, L. (2000) High-level neuronal expression of abeta 1-42 in wild-type human amyloid protein precursor transgenic mice: synaptotoxicity without plaque formation. *J. Neurosci.*, **20**, 4050–4058.
31. Xie, Y., Zhou, B., Lin, M.Y., Wang, S., Foust, K.D. and Sheng, Z.H. (2015) Endolysosomal deficits augment mitochondria pathology in spinal motor neurons of asymptomatic fALS mice. *Neuron*, **87**, 355–370.
32. Bhalla, A., Vetanovetz, C.P., Morel, E., Chamoun, Z., Di Paolo, G. and Small, S.A. (2012) The location and trafficking routes of the neuronal retromer and its role in amyloid precursor protein transport. *Neurobiol. Dis.*, **47**, 126–134.
33. Choy, R.W., Park, M., Temkin, P., Herring, B.E., Marley, A., Nicoll, R.A. and von Zastrow, M. (2014) Retromer mediates a discrete route of local membrane delivery to dendrites. *Neuron*, **82**, 55–62.
34. Tammineni, P., Ye, X., Feng, T., Aikal, D. and Cai, Q. (2017) Impaired retrograde transport of axonal autophagosomes contributes to autophagic stress in Alzheimer's disease neurons. *Elife*, **6**.
35. Bingol, B., Tea, J.S., Phu, L., Reichelt, M., Bakalarski, C.E., Song, Q., Foreman, O., Kirkpatrick, D.S. and Sheng, M. (2014) The mitochondrial deubiquitinase USP30 opposes parkin-mediated mitophagy. *Nature*, **510**, 370–375.
36. Katayama, H., Kogure, T., Mizushima, N., Yoshimori, T. and Miyawaki, A. (2011) A sensitive and quantitative technique for detecting autophagic events based on lysosomal delivery. *Chem. Biol.*, **18**, 1042–1052.
37. Gowrishankar, S., Yuan, P., Wu, Y., Schrag, M., Paradise, S., Grutzendler, J., De Camilli, P. and Ferguson, S.M. (2015) Massive accumulation of luminal protease-deficient axonal lysosomes at Alzheimer's disease amyloid plaques. *Proc. Natl. Acad. Sci. USA*, **112**, E3699–E3708.
38. Mecozzi, V.J., Berman, D.E., Simoes, S., Vetanovetz, C., Awal, M.R., Patel, V.M., Schneider, R.T., Petsko, G.A., Ringe, D. and Small, S.A. (2014) Pharmacological chaperones stabilize retromer to limit APP processing. *Nat. Chem. Biol.*, **10**, 443–449.
39. Wassmer, T., Attar, N., Harterink, M., van Weering, J.R., Traer, C.J., Oakley, J., Goud, B., Stephens, D.J., Verkade, P., Korswagen, H.C. *et al.* (2009) The retromer coat complex coordinates endosomal sorting and dynein-mediated transport, with carrier recognition by the trans-Golgi network. *Dev. Cell.*, **17**, 110–122.
40. Hong, Z., Yang, Y., Zhang, C., Niu, Y., Li, K., Zhao, X. and Liu, J.J. (2009) The retromer component SNX6 interacts with dynactin p150(Glued) and mediates endosome-to-TGN transport. *Cell Res.*, **19**, 1334–1349.
41. Wang, C.L., Tang, F.L., Peng, Y., Shen, C.Y., Mei, L. and Xiong, W.C. (2012) VPS35 regulates developing mouse hippocampal neuronal morphogenesis by promoting retrograde trafficking of BACE1. *Biol. Open.*, **1**, 1248–1257.
42. Tammineni, P. and Cai, Q. (2017) Defective retrograde transport impairs autophagic clearance in Alzheimer disease neurons. *Autophagy*, **13**, 982–984.
43. Nixon, R.A. and Yang, D.S. (2011) Autophagy failure in Alzheimer's disease–locating the primary defect. *Neurobiol. Dis.*, **43**, 38–45.
44. Nixon, R.A. (2013) The role of autophagy in neurodegenerative disease. *Nat. Med.*, **19**, 983–997.
45. Maday, S. and Holzbaur, E.L. (2016) Compartment-specific regulation of autophagy in primary neurons. *J. Neurosci.*, **36**, 5933–5945.
46. Cheng, X.T., Zhou, B., Lin, M.Y., Cai, Q. and Sheng, Z.H. (2015) Axonal autophagosomes recruit dynein for retrograde transport through fusion with late endosomes. *J. Cell. Biol.*, **209**, 377–386.
47. Maday, S., Wallace, K.E. and Holzbaur, E.L. (2012) Autophagosomes initiate distally and mature during transport toward the cell soma in primary neurons. *J. Cell. Biol.*, **196**, 407–417.
48. Yu, W.H., Cuervo, A.M., Kumar, A., Peterhoff, C.M., Schmidt, S.D., Lee, J.H., Mohan, P.S., Mercken, M., Farmery, M.R., Tjernberg, L.O. *et al.* (2005) Macroautophagy – a novel Beta-amyloid peptide-generating pathway activated in Alzheimer's disease. *J. Cell. Biol.*, **171**, 87–98.
49. Yang, D.S., Stavrides, P., Mohan, P.S., Kaushik, S., Kumar, A., Ohno, M., Schmidt, S.D., Wesson, D., Bandyopadhyay, U., Jiang, Y. *et al.* (2011) Reversal of autophagy dysfunction in the TgCRND8 mouse model of Alzheimer's disease ameliorates amyloid pathologies and memory deficits. *Brain*, **134**, 258–277.
50. Braak, H. and Braak, E. (1991) Demonstration of amyloid deposits and neurofibrillary changes in whole brain sections. *Brain Pathol.*, **1**, 213–216.
51. Cai, Q., Zakaria, H.M., Simone, A. and Sheng, Z.H. (2012) Spatial parkin translocation and degradation of damaged mitochondria via mitophagy in live cortical neurons. *Curr Biol.*, **22**, 545–552.
52. Gibson, G.E. and Shi, Q. (2010) A mitocentric view of Alzheimer's disease suggests multi-faceted treatments. *J. Alzheimers Dis.*, **20**, S591–S607.
53. Banker, G.A. and Cowan, W.M. (1979) Further observations on hippocampal neurons in dispersed cell culture. *J. Comp. Neurol.*, **187**, 469–493.
54. Kang, J.S., Tian, J.H., Pan, P.Y., Zald, P., Li, C., Deng, C. and Sheng, Z.H. (2008) Docking of axonal mitochondria by syntaphilin controls their mobility and affects short-term facilitation. *Cell*, **132**, 137–148.
55. Zhou, B., Cai, Q., Xie, Y. and Sheng, Z.H. (2012) Snapin recruits dynein to BDNF-TrkB signaling endosomes for retrograde axonal transport and is essential for dendrite growth of cortical neurons. *Cell Rep.*, **2**, 42–51.